JOURNAL OF BACTERIOLOGY, Dec. 2008, p. 7904–7909 Vol. 190, No. 24
0021-9193/08/$08.00+0 doi:10.1128/JB.01116-08

Direct Observation of *Staphylococcus aureus* Cell Wall Digestion by Lysostaphin▽

Grégory Francius,[1] Oscar Domenech,[2] Marie Paule Mingeot-Leclercq,[2] and Yves F. Dufrêne[1]*

Unité de Chimie des Interfaces, Université Catholique de Louvain, Croix du Sud 2/18, B-1348 Louvain-la-Neuve, Belgium,[1] and Unité de Pharmacologie Cellulaire et Moléculaire, Université Catholique de Louvain, Avenue E. Mounier 73, B-1200 Brussels, Belgium[2]

Received 8 August 2008/Accepted 25 September 2008

The advent of *Staphylococcus aureus* strains that are resistant to virtually all antibiotics has increased the need for new antistaphylococcal agents. An example of such a potential therapeutic is lysostaphin, an enzyme that specifically cleaves the *S. aureus* peptidoglycan, thereby lysing the bacteria. Here we tracked over time the structural and physical dynamics of single *S. aureus* cells exposed to lysostaphin, using atomic force microscopy. Topographic images of native cells revealed a smooth surface morphology decorated with concentric rings attributed to newly formed peptidoglycan. Time-lapse images collected following addition of lysostaphin revealed major structural changes in the form of cell swelling, splitting of the septum, and creation of nanoscale perforations. Notably, treatment of the cells with lysostaphin was also found to decrease the bacterial spring constant and the cell wall stiffness, demonstrating that structural changes were correlated with major differences in cell wall nanomechanical properties. We interpret these modifications as resulting from the digestion of peptidoglycan by lysostaphin, eventually leading to the formation of osmotically fragile cells. This study provides new insight into the lytic activity of lysostaphin and offers promising prospects for the study of new antistaphylococcal agents.

The gram-positive bacterium *Staphylococcus aureus* is a versatile pathogen capable of causing a wide range of human diseases (23, 28). Peptidoglycan, the major cell wall components of *S. aureus*, is known to be the target of important antibiotics (22, 39). Among these, β-lactams (e.g., penicillins) exert their antimicrobial activity by interfering with the enzymes (penicillin binding proteins) specifically involved in peptidoglycan synthesis, while glycopeptides (e.g., vancomycin) bind with high affinity and specificity to peptidoglycan precursors, thereby preventing their incorporation into the bacterial cell wall (38). Currently, there is a constant need for new antistaphylococcal drugs owing to the development of antibiotic-resistant strains (4, 38, 39). An example of such a novel drug is lysostaphin, an enzyme secreted by *Staphylococcus simulans* which specifically cleaves the peptidoglycan cross-linking pentaglycine bridges of *S. aureus*, thereby hydrolyzing the cell wall and lysing the bacteria (7, 27, 33). Due to its unique specificity, lysostaphin could have high potential in the treatment of antibiotic-resistant staphylococcal infections (27). For instance, lysostaphin, given alone or in combination with vancomycin, was shown to be more effective in the treatment of experimental methicillin-resistant *S. aureus* aortic valve endocarditis than vancomycin alone (9). Lysostaphin was also reported to be effective in the treatment of eye infections caused by *S. aureus* (12).

Knowledge of the molecular mechanisms underlying peptidoglycan digestion by lysostaphin is a key toward its efficient use in antistaphylococcal therapies. Early structural investigations using electron microscopy revealed that *S. aureus* cells exposed to lysostaphin showed perforations and more extensive damage, including the separation of walls from the plasma membranes and the disintegration of large sections of the walls (34). As a consequence, most cells exposed to the enzyme were rendered osmotically fragile. Among these, cells that retain the capacity to revert to normal staphylococci were designated spheroplasts, as opposed to protoplasts, in which the whole cell wall was digested away. Although powerful, electron microscopy techniques are not suited for tracking dynamic, time-dependent processes on single cells, and they cannot probe the cell wall mechanical properties.

Recently, atomic force microscopy (AFM) (20, 30) has provided new opportunities for studying microbial cell walls at the single-cell and single-molecule levels (14, 15). The technique is particularly well-suited for visualizing the surfaces of single live cells while they grow (11, 31, 37), yielding information on cell wall assembly and dynamics that cannot be obtained with traditional microscopies. For instance, Touhami et al. (37) were able to monitor cell growth and division events in *S. aureus* using AFM combined with thin-section transmission electron microscopy. Nanoscale holes were seen around the septal annulus at the onset of division and were attributed to cell wall structures possessing high autolytic activity. After cell separation, concentric rings were observed on the surface of the new cell wall and were suggested to reflect newly formed peptidoglycan. AFM can also be used to study the effect of drugs on microbial cell walls. In one such study, mycobacteria were observed prior to and after incubation with isoniazid, ethionamide, ethambutol, or streptomycin (1). Upon drug treatment, major structural alterations were observed in the form of layered structures, striations, and porous morphologies, suggesting that they reflect the inhibition of the synthesis of three

* Corresponding author. Mailing address: Unité de Chimie des Interfaces, Université Catholique de Louvain, Croix du Sud 2/18, B-1348 Louvain-la-Neuve, Belgium. Phone: (32) 10 47 36 00. Fax: (32) 10 47 20 05. E-mail: yves.dufrene@uclouvain.be.

▽ Published ahead of print on 3 October 2008.

major cell wall constituents, i.e., mycolic acids, arabinans, and proteins.

Here, we used AFM to track the structural and physical dynamics of single *S. aureus* cells exposed to lysostaphin. AFM images show that the enzyme causes substantial swelling of the cells, favors splitting of the septum, and induces the creation of nanoscale perforations. Consistent with this, nanomechanical measurements demonstrate that these structural changes correlate with a major decrease of bacterial turgor pressure and cell wall stiffness, reflecting the formation of osmotically fragile cells.

MATERIALS AND METHODS

Bacterial strain and growth conditions. *Staphylococcus aureus* (methicillin-susceptible *S. aureus* strain ATCC 25923; American Type Culture Collection [ATCC], Manassas, VA) was grown in Mueller-Hinter broth (Becton Dickinson, France) to mid-exponential growth phase (optical density at 600 nm = 0.6) at 37°C with continuous stirring. Cells were centrifuged (7,000 rpm for 10 min) and washed twice by resuspension in phosphate-buffered saline (PBS) and centrifugation.

AFM measurements. AFM images and force-distance curves were recorded in PBS solution (10 mM PBS, 150 mM NaCl, pH 7.4) at room temperature, using a Nanoscope IV multimode AFM (Veeco Metrology Group, Santa Barbara, CA). Cells were immobilized by mechanical trapping into porous polycarbonate membranes (Millipore) with a pore size similar to the bacterial cell size (13, 26). After a concentrated cell suspension was filtered, the filter was gently rinsed with PBS, carefully cut (1 cm by 1 cm), and attached to a steel sample puck (Veeco Metrology Group) using a small piece of double-face adhesive tape, and the mounted sample was transferred into the AFM liquid cell while avoiding dewetting. The spring constants of the cantilevers were measured using the thermal noise method (Picoforce; Veeco Metrology Group), yielding a mean value of 0.0255 ± 0.001 N/m. For lysostaphin experiments, PBS solutions containing 16 μg/ml lysostaphin from *S. simulans* (Sigma, Belgium) were injected into the AFM liquid cell.

Mechanical properties were measured by recording arrays of 32-by-32 force curves, using a maximum applied force of 1.75 to 2 nN to avoid sample damage. The bacterial spring constant, k_b, was determined from the slope of the linear portions of the curves for raw deflection (nm) versus piezo displacement (nm) (5): $k_b = (k_C \cdot s)/(1 - s)$, where k_C is the spring constant of the cantilever and s the observed slope. The bacterial Young modulus was obtained by fitting the curves for force versus indentation using the Hertz model with a conical (tip)-plane (cell surface) geometry (24): $F = \{2E\tan\alpha/[\pi(1 - \nu^2)]\} \cdot \delta^2$, where F is the force, δ is the indentation depth, E is the Young modulus, ν is the Poisson coefficient, and α is the semi-top angle of the tip. This simple model is valid for elastic surfaces and does not take into account tip-surface adhesion. The latter assumption is reasonable since adhesion forces were negligible in the present study. The mathematical analysis was performed with an automatic Fortran C++ algorithm as described elsewhere (16, 17).

RESULTS AND DISCUSSION

High-resolution imaging of *S. aureus*. Cells immobilized in porous membranes were imaged in buffer solution. A representative low-resolution deflection image of a single cell is shown in Fig. 1A. Due to the large curvature of the specimen, height images had fairly poor resolution while deflection images were much more sensitive to the surface relief. Using small imaging forces (~100 pN), images of the same area were obtained repeatedly without detaching the cell or significantly altering the surface morphology. The cell, located at the center of the image, was surrounded by artifactual features resulting from the contact between the AFM tip and the pore edges. The cell surface was smooth and showed circular or concentric rings enclosing a central depression. The high-resolution height image recorded on top of the cell, shown in Fig. 1B, reveals that the rings were separated by 20 to 50 nm. These

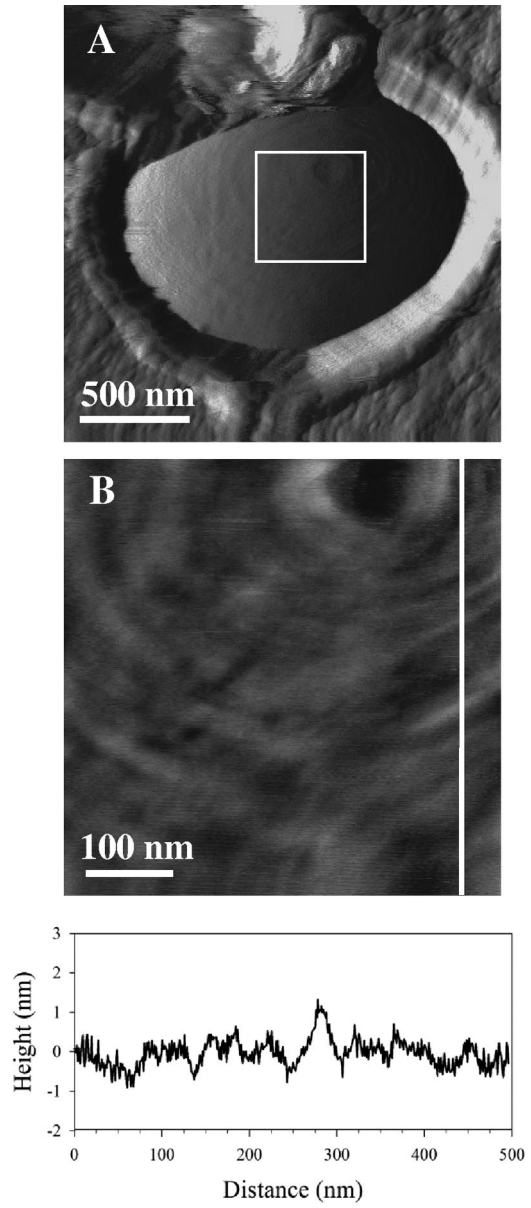

FIG. 1. Imaging of single *S. aureus* cells. (A) Low-resolution deflection image recorded in PBS, showing a single cell trapped in a pore of the polycarbonate membrane. (B) High-resolution height image recorded in the square region highlighted in panel A, together with a vertical cross-section taken along the white line.

features are similar to those reported earlier by Touhami et al. (37), who observed concentric rings on the newly formed cell walls of *S. aureus* cells but not on older regions of the cell walls. The ring structures are also reminiscent of the circular patterns seen by several groups using electron microscopy techniques (2, 3, 6, 21, 22). We therefore conclude that the rings reflect structural features of the peptidoglycan strands found on the surface of the new wall after daughter cells have separated. As pointed out by Touhami et al. (37), the concentricity of the rings implies that the peptidoglycan strands are themselves oriented in a similar fashion and are added or removed in an orderly manner. Note that a number of cells did not show any

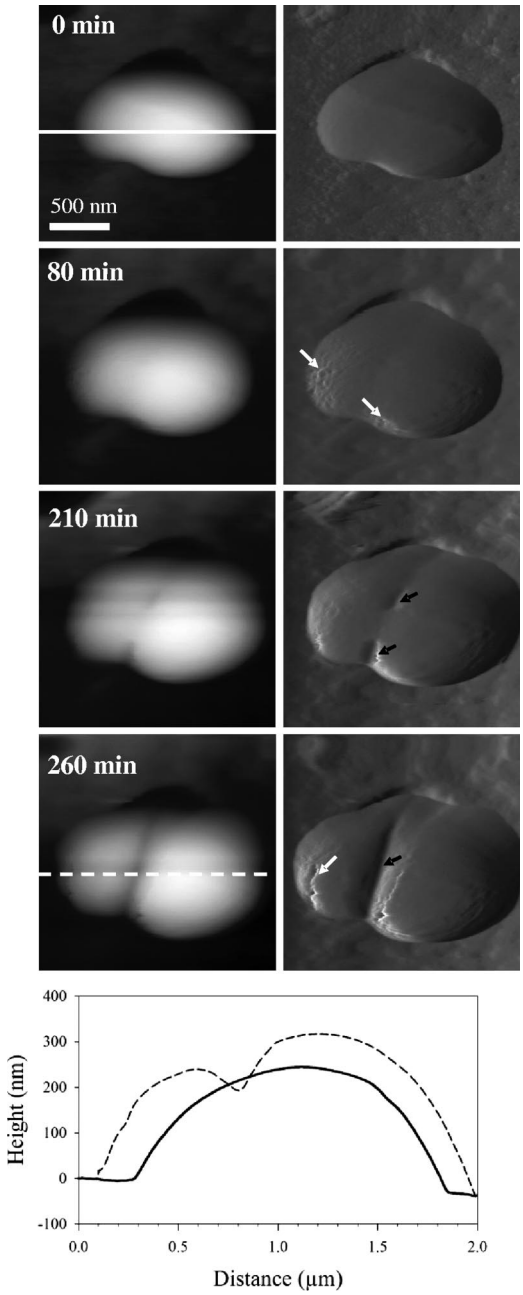

FIG. 2. Imaging of single *S. aureus* cells following incubation with lysostaphin. A series of height (left) and deflection (right) images recorded in real time for a single cell prior to and after incubation with 16 μg/ml lysostaphin in PBS for 80, 210, and 260 min is shown. The lower panel compares vertical cross-sections taken at 0 min (continuous line) and 260 min (dashed line). White arrows show nanoscale perforations enlarging with time, while black arrows show splitting of the septum. Similar data were obtained with different cells from four independent cultures.

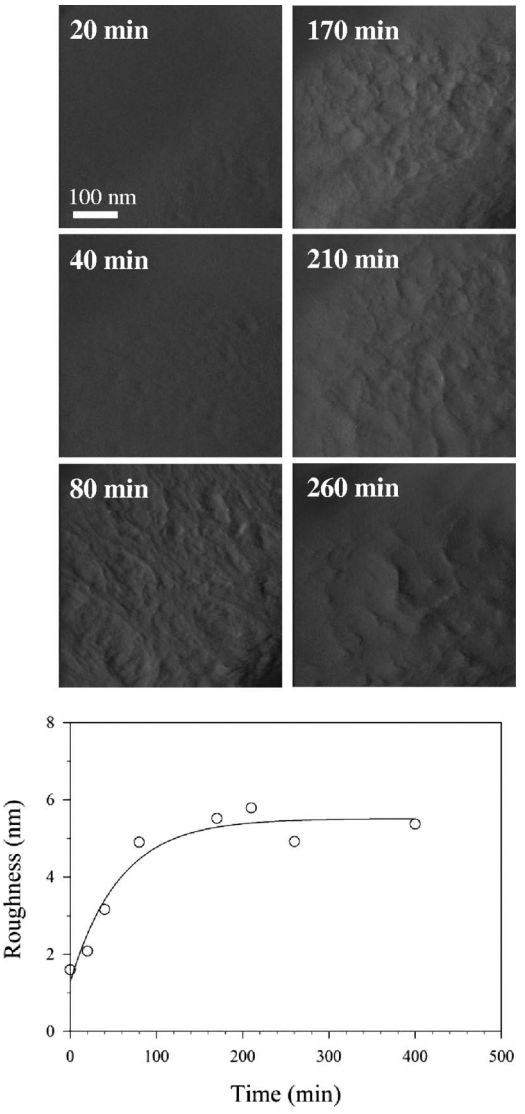

FIG. 3. Imaging of lysostaphin-treated cells at high resolution. A series of deflection images recorded on top of a single cell after incubation with 16 μg/ml lysostaphin for 20, 40, 80, 170, 210, and 260 min is shown. The lower panel shows the temporal evolution of the root mean square roughness measured on height images.

ring structures, presumably because their surfaces consisted of older cell wall material (Fig. 2, upper panels).

Lysostaphin induces major structural alterations. Peptidoglycan is an important component of the *S. aureus* cell wall, conferring strength and rigidity to the cell, allowing growth and division, maintaining cell shape, and protecting against osmotic lysis (8, 21). In *S. aureus* and other gram-positive bacteria, where the external membrane is absent, the multilayered peptidoglycan represents the limit of the cell and therefore the site for exchanges and interactions with the outside environment (10). In particular, peptidoglycan is known to be an important target for antimicrobial compounds (35), including lysostaphin, which hydrolyzes the pentapeptide cross-linkages (27).

With this in mind, we used in situ AFM imaging to observe structural changes on single *S. aureus* cells exposed to lysostaphin. Figure 2 shows height and deflection images recorded for the same cell following incubation with 16 μg/ml lysostaphin for 0, 80, 210, and 260 min. As can be seen in the vertical cross-sections, a significant increase in cell size was noted over the course of the experiment, with the cell height increasing by ~100 nm after 260 min. In agreement with early

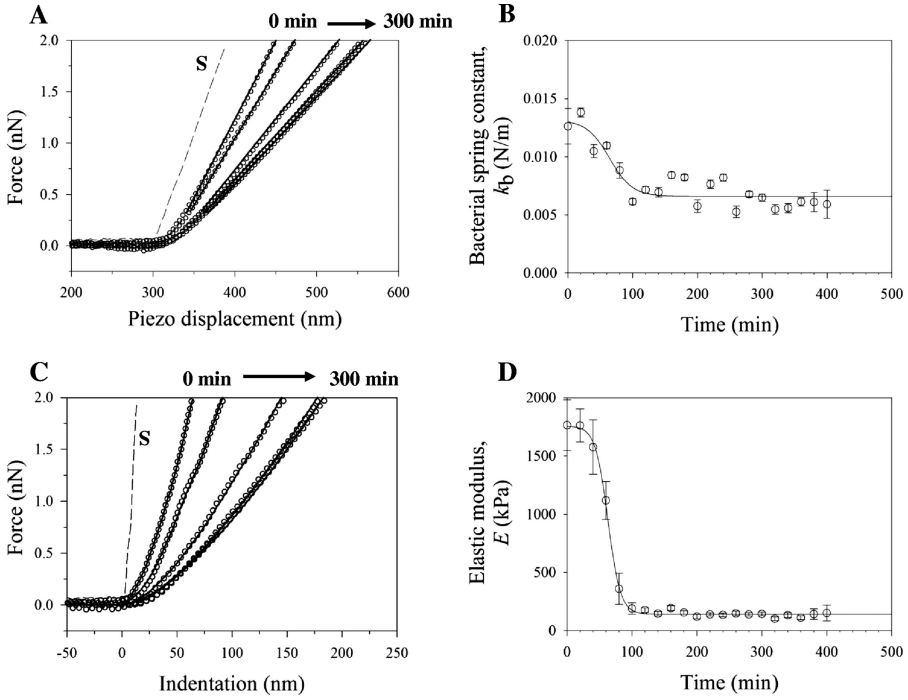

FIG. 4. Mechanical properties of native and lysostaphin-treated cells. (A) Representative force-versus-displacement curves recorded on the polymer support (dashed line, S) and on a single cell prior to (0 min) and after (20, 60, 100, and 300 min) incubation with lysostaphin at 16 μg/ml. Open symbols are the raw data, while the solid lines show the theoretical fit (Hooke's law) used to extract the bacterial spring constant. (B) Evolution of the bacterial spring constant as a function of incubation time. Each data point represents the mean and standard deviation of 1,024 measurements obtained at different locations in the same cell. (C) Force-indentation curves obtained from the curves shown in panel A. Open symbols show the data, while the solid lines show the theoretical fits (Hertz model) used to extract the Young modulus values. (D) Evolution of the Young modulus as a function of incubation time. Each data point represents the mean and standard deviation of 1,024 measurements obtained at different locations in the same cell. Similar behaviors were observed for six different cells using two different tips.

viability studies (25, 34), we interpret such cell swelling as evidence for the formation of lysostaphin-induced osmotically fragile cells, resulting from peptidoglycan hydrolysis.

Moreover, progressive alteration of the cell surface structure was clearly observed after lysostaphin addition. After 80 min, nanoscale perforations were seen, which were about 50 to 100 nm in diameter and 25 to 75 nm in depth (Fig. 2). With time (e.g., after 260 min), these holes enlarged until they merged together to form larger perforations. These structures are reminiscent of the small depressions seen at the onset of division (37) and may reflect so-called murosomes (22), i.e., regions of the cell wall having high autolytic activity. Interestingly, splitting of the septum was observed after 210 min (Fig. 2). We note that these features, i.e., perforations and splitting of the septum, were never observed when cells were imaged in PBS in the absence of lysostaphin, even for prolonged periods of time (up to 240 min), confirming that they result from the lytic activity of the enzyme. It is also worth mentioning that protoplasts in which the cell wall had been completely digested could never be observed by AFM, most likely because they were immediately ruptured by the scanning tip. Besides localized surface modifications, we also found that lysostaphin increased the cell surface roughness (Fig. 3). Power spectral density analysis of the fast Fourier transform of height images revealed that the root mean square roughness for native and treated cells increased with the length scale to reach a plateau after 200 nm. Notably, the roughness on 500-nm by 500-nm height images increased from 1.6 ± 0.3 nm for untreated cells to 5.4 ± 1.2 nm for cells treated for 200 min (Fig. 3). These results are qualitatively consistent with earlier electron microscopy investigations (34) showing progressive disintegration of the cell wall and separation from the plasma membrane after exposure to lysostaphin.

Taken together, our AFM images demonstrate that incubation of *S. aureus* with lysostaphin causes substantial swelling of the cell body, favors splitting of the septum, induces nanoscale perforations, and increases the cell surface roughness. Presumably, these time-dependent cell wall modifications result from peptidoglycan digestion, eventually leading to the formation of osmotically fragile spheroplasts.

Lysostaphin alters the cell wall mechanical properties. In view of the role of peptidoglycan in providing rigidity and protection against osmotic lysis, we then addressed the pertinent question as to whether the observed structural changes were correlated with differences in cell wall mechanical properties. To this end, cells incubated with lysostaphin were probed using nanoindentation measurements (Fig. 4 and 5). Figure 4A shows typical force-versus-piezo displacement curves obtained for the polymer support and for a single cell at increasing incubation times. Consistent with the work of Gaboriaud et al. (18), the curves recorded on the cell surface showed two domains, i.e., a nonlinear domain at low loading forces followed by a linear one at high loading forces. From the shape of these curves, it can be seen that the cell wall was

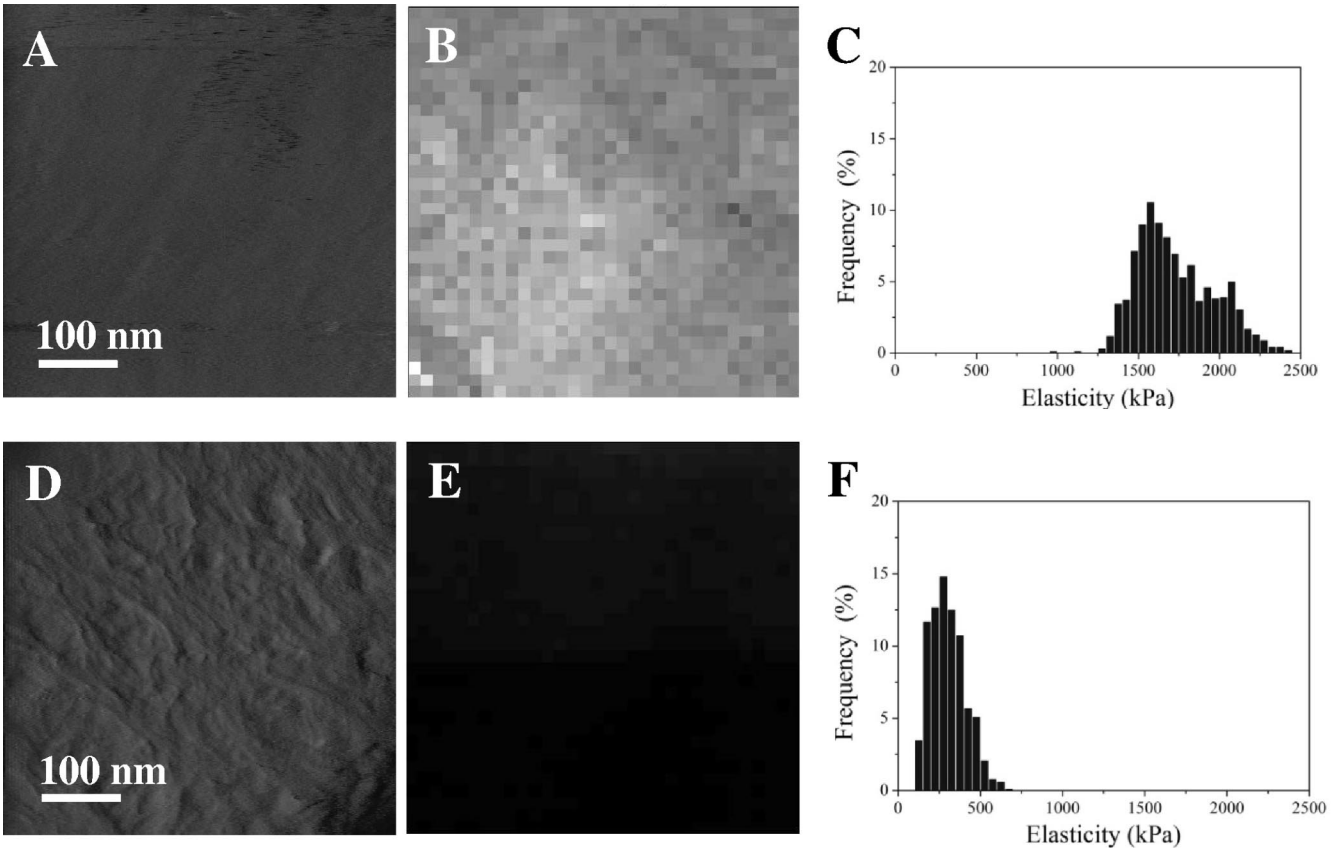

FIG. 5. Mapping of cell surface elasticity. (A and D) High-resolution deflection images recorded for an *S. aureus* cell prior to and after incubation with lysostaphin for 80 min. (B and E) Elasticity maps (z-range = 3,000 kPa). (C and F) Distribution of elasticity values (n = 1,024 force curves) corresponding to the elasticity maps.

already substantially softer than the support and that lysostaphin caused a progressive softening of the cell wall.

To provide quantitative information on the cell wall mechanical properties, two parameters were extracted from the force curves, i.e., the bacterial spring constant, which is related to the inner turgor pressure of the cell (5, 18, 19, 40), and the Young modulus, which reflects cell surface elasticity (17, 18, 29, 36). Bacterial spring constant values, k_b, were determined from the slopes of the linear portions of the force-versus-piezo displacement curves (Fig. 4A). The k_b value of native cells was found to be 0.013 ± 0.001 N/m (Fig. 4B), which agrees reasonably well with values reported earlier for six *Lactobacillus* strains (0.016 to 0.053 N/m) (32). Our slightly lower values could be due to the higher ionic strength that we used or to differences in the cell wall organization. Notably, incubation with lysostaphin caused a progressive decrease of k_b, from 0.013 ± 0.001 N/m to 0.006 ± 0.001 N/m after 100 min of exposure. This change may be attributed to a decrease of the inner turgor pressure of the cell (5, 18, 19, 40), in agreement with the observed cell swelling (Fig. 2) and with the notion that lysostaphin generates osmotically fragile cells.

Next, we estimated Young modulus values by converting the force curves into force-indentation curves and analyzing them using the Hertz theory (Fig. 4C). Figure 4D shows that within 100 min, the Young modulus of the cells decreased from 1,764 ± 218 kPa to 189 ± 49 kPa, demonstrating that lysostaphin induces a dramatic reduction of cell wall stiffness. This finding is fully consistent with the mode of action of the enzyme, which cleaves the peptidoglycan cross-linking pentaglycine bridges. Also of note is the comparison between the level of indentation and cell swelling: for a constant force of 1 nN, the difference in indentation depth (for native cells versus cells treated for 300 min) was ~100 nm, which is on the order of the height increase observed in the images (Fig. 2). Finally, arrays of 32-by-32 force curves were recorded across the cell surface to map local variations of elasticity. As shown in Fig. 5, elasticity maps on native and treated cells showed rather uniform contrasts, reflecting homogeneous distributions of elasticity. The homogeneously dark contrast observed after 80 min confirmed that the entire cell wall was softened upon treatment with the enzyme.

In conclusion, we have observed, for the first time in situ and on a nanoscale, the digestion of the *S. aureus* cell wall by lysostaphin, revealing that the enzyme causes substantial swelling of the cells and major alterations of their surface structure (septum splitting, nanoscale perforations, and increased roughness). Using force measurements, we also showed that these structural changes correlate with major differences in mechanical properties, i.e., with a decrease of bacterial turgor pressure and of cell wall stiffness. This study shows that AFM is a promising tool for exploring the organization and assembly of peptidoglycan and for investigating its interactions with enzymes and drugs.

ACKNOWLEDGMENTS

This work was supported by the National Foundation for Scientific Research (FNRS); the Université Catholique de Louvain (Fonds Spéciaux de Recherche); the Federal Office for Scientific, Technical and Cultural Affairs (Interuniversity Poles of Attraction Programme); and the Research Department of the Communauté Française de Belgique (Concerted Research Action). Y.F.D. is a research associate at the FNRS.

REFERENCES

1. **Alsteens, D., C. Verbelen, E. Dague, D. Raze, A. R. Baulard, and Y. F. Dufrêne.** 2008. Organization of the mycobacterial cell wall: a nanoscale view. Pflugers Arch. **456:**117–125.
2. **Amako, K., and A. Umeda.** 1977. Scanning electron microscopy of *Staphylococcus*. J. Ultrastruct. Res. **58:**34–40.
3. **Amako, K., A. Umeda, and K. Murata.** 1982. Arrangement of peptidoglycan in the cell wall of *Staphylococcus* spp. J. Bacteriol. **150:**844–850.
4. **Appelbaum, P. C., and B. Bozdogan.** 2004. Vancomycin resistance in *Staphylococcus aureus*. Clin. Lab. Med. **24:**381–402.
5. **Arnoldi, M., M. Fritz, E. Bauerlein, M. Radmacher, E. Sackmann, and A. Boulbitch.** 2000. Bacterial turgor pressure can be measured by atomic force microscopy. Phys. Rev. E **62:**1034–1044.
6. **Beveridge, T. J.** 1999. The ultrastructure of gram-positive cell walls, p. 3–10. *In* V. Fischetti, R. Novick, J. Ferretti, D. Portnoy, and J. Rood (ed.), Gram-positive pathogens. ASM Press, Washington, DC.
7. **Browder, H. P., W. A. Zygmunt, J. R. Young, and P. A. Tavormina.** 1965. Lysostaphin: enzymatic mode of action. Biochem. Biophys. Res. Commun. **19:**383–389.
8. **Cabeen, M. T., and C. Jacobs-Wagner.** 2005. Bacterial cell shape. Nat. Rev. Microbiol. **3:**601–610.
9. **Climo, M. W., R. L. Patron, B. P. Goldstein, and G. L. Archer.** 1998. Lysostaphin treatment of experimental methicillin-resistant *Staphylococcus aureus* aortic valve endocarditis. Antimicrob. Agents Chemother. **42:**1355–1360.
10. **Cloud-Hansen, K. A., S. B. Peterson, E. V. Stabb, W. E. Goldman, M. J. McFall-Ngai, and J. Handelsman.** 2006. Breaching the great wall: peptidoglycan and microbial interactions. Nat. Rev. Microbiol. **4:**710–716.
11. **Dague, E., D. Alsteens, J. P. Latgé, and Y. F. Dufrêne.** 2008. High-resolution cell surface dynamics of germinating *Aspergillus fumigatus* conidia. Biophys. J. **94:**656–660.
12. **Dajcs, J. J., B. A. Thibodeaux, E. B. Hume, X. Zheng, G. D. Sloop, and R. J. O'Callaghan.** 2001. Lysostaphin is effective in treating methicillin-resistant *Staphylococcus aureus* endophthalmitis in the rabbit. Curr. Eye Res. **22:**451–457.
13. **Dufrêne, Y. F., C. J. P. Boonaert, P. A. Gerin, M. Asther, and P. G. Rouxhet.** 1999. Direct probing of the surface ultrastructure and molecular interactions of dormant and germinating spores of *Phanerochaete chrysosporium*. J. Bacteriol. **181:**5350–5354.
14. **Dufrêne, Y. F.** 2004. Using nanotechniques to explore microbial surfaces. Nat. Rev. Microbiol. **2:**451–460.
15. **Dufrêne, Y. F.** 2008. Towards nanomicrobiology using atomic force microscopy. Nat. Rev. Microbiol. **6:**674–680.
16. **Francius, G., J. Hemmerle, V. Ball, P. Lavalle, C. Picart, J. C. Voegel, P. Schaaf, and B. Senger.** 2007. Stiffening of soft polyelectrolyte architectures by multilayer capping evidenced by viscoelastic analysis of AFM indentation measurements. J. Phys. Chem. C **111:**8299–8306.
17. **Francius, G., B. Tesson, E. Dague, V. Martin-Jezequel, and Y. F. Dufrêne.** 2008. Nanostructure and nanomechanics of live *Phaeodactylum tricornutum* morphotypes. Environ. Microbiol. **10:**1344–1356.
18. **Gaboriaud, F., S. Bailet, E. Dague, and F. Jorand.** 2005. Surface structure and nanomechanical properties of *Shewanella putrefaciens* bacteria at two pH values (4 and 10) determined by atomic force microscopy. J. Bacteriol. **187:**3864–3868.
19. **Gaboriaud, F., M. L. Gee, R. Strugnell, and J. F. Duval.** 2008. Coupled electrostatic, hydrodynamic, and mechanical properties of bacterial interfaces in aqueous media. Langmuir **24:**10988–10995.
20. **Gerber, C., and H. P. Lang.** 2006. How the doors to the nanoworld were opened. Nat. Nanotechnol. **1:**3–5.
21. **Giesbrecht, P., H. Labischinski, and J. Wecke.** 1985. A special morphogenetic wall defect and the subsequent activity of murosomes as the very reason for penicillin-induced bacteriolysis in *Staphylococci*. Arch. Microbiol. **141:**315–324.
22. **Giesbrecht, P., T. Kersten, H. Maidhof, and J. Wecke.** 1998. Staphylococcal cell wall: morphogenesis and fatal variations in the presence of penicillin. Microbiol. Mol. Biol. Rev. **62:**1371–1414.
23. **Gordon, R. J., and F. D. Lowy.** 2008. Pathogenesis of methicillin-resistant *Staphylococcus aureus* infection. Clin. Infect. Dis. **46:**S350–S359.
24. **Hertz, H.** 1881. Ueber die Berührung fester elastischer Körper. J. Reine Angew. Math. **92:**156–171.
25. **Huber, T. W., and V. T. Schuhardt.** 1970. Lysostaphin-induced, osmotically fragile *Staphylococcus aureus* cells. J. Bacteriol. **103:**116–119.
26. **Kasas, S., and A. Ikai.** 1995. A method for anchoring round shaped cells for atomic-force microscope imaging. Biophys. J. **68:**1678–1680.
27. **Kumar, J. K.** 2008. Lysostaphin: an antistaphylococcal agent. Appl. Microbiol. Biotechnol. **80:**555–561.
28. **Lowy, F. D.** 1998. *Staphylococcus aureus* infections. N. Engl. J. Med. **339:**520–532.
29. **Matzke, R., K. Jacobson, and M. Radmacher.** 2001. Direct, high-resolution measurement of furrow stiffening during division of adherent cells. Nat. Cell Biol. **3:**607–610.
30. **Muller, D. J., and Y. F. Dufrêne.** 2008. Atomic force microscopy as a multifunctional molecular toolbox in nanobiotechnology. Nat. Nanotechnol. **3:**261–269.
31. **Plomp, M., T. J. Leighton, K. E. Wheeler, H. D. Hill, and A. J. Malkin.** 2007. *In vitro* high-resolution structural dynamics of single germinating bacterial spores. Proc. Natl. Acad. Sci. USA **104:**9644–9649.
32. **Schar-Zammaretti, P., and J. Ubbink.** 2003. The cell wall of lactic acid bacteria: surface constituents and macromolecular conformations. Biophys. J. **85:**4076–4092.
33. **Schindler, C. A., and V. T. Schuhardt.** 1964. Lysostaphin: a new bacteriolytic agent for the *Staphylococcus*. Proc. Natl. Acad. Sci. USA **51:**414–421.
34. **Schuhardt, V. T., T. W. Huber, and L. M. Pope.** 1969. Electron microscopy and viability of lysostaphin-induced staphylococcal spheroplasts, protoplast-like bodies, and protoplasts. J. Bacteriol. **97:**396–401.
35. **Silver, L. L.** 2003. Novel inhibitors of bacterial cell wall synthesis. Curr. Opin. Microbiol. **6:**431–438.
36. **Touhami, A., B. Nysten, and Y. F. Dufrêne.** 2003. Nanoscale mapping of the elasticity of microbial cells by atomic force microscopy. Langmuir **19:**4539–4543.
37. **Touhami, A., M. H. Jericho, and T. J. Beveridge.** 2004. Atomic force microscopy of cell growth and division in *Staphylococcus aureus*. J. Bacteriol. **186:**3286–3295.
38. **Walsh, C.** 2000. Molecular mechanisms that confer antibacterial drug resistance. Nature **406:**775–781.
39. **Walsh, C.** 2003. Where will new antibiotics come from? Nat. Rev. Microbiol. **1:**65–70.
40. **Yao, X., J. Walter, S. Burke, S. Stewart, M. H. Jericho, D. Pink, R. Hunter, and T. J. Beveridge.** 2002. Atomic force microscopy and theoretical considerations of surface properties and turgor pressures of bacteria. Colloids Surf. B **23:**213–230.